VERSITA

Cent. Eur. J. Chem. • 10(1) • 2012 • 256-266
DOI: 10.2478/s11532-011-0137-0

Central European Journal of **Chemistry**

Oxidative addition of methyl iodide to [Rh(PhCOCHCOPh)(CO)(P(OCH$_2$)$_3$CCH$_3$)]: an experimental and computational study

Research Article

Johannes J. C. Erasmus[1], Jeanet Conradie[1,2*]

[1]*Department of Chemistry, PO Box 339, University of the Free State, 9300 Bloemfontein, Republic of South Africa*

[2]*Department of Chemistry and Centre for Theoretical and Computational Chemistry, University of Tromsø, N-9037 Tromsø, Norway*

Received 30 June 2011; Accepted 7 October 2011

Abstract: The reaction rate of the oxidative addition and CO insertion steps of methyl iodide with [Rh(PhCOCHCOPh)(CO)(P(OCH$_2$)$_3$CCH$_3$)] are presented. Large negative experimental values for the activation entropy and results from a density functional theory computational chemistry study indicated *trans* addition of the CH$_3$I to [Rh(PhCOCHCOPh)(CO)(P(OCH$_2$)$_3$CCH$_3$)]. A study of the molecular orbitals gives insight into the flow of electrons during the oxidative addition reaction. CO insertion leads to a square pyramidal [Rh(PhCOCHCOPh)(P(OCH$_2$)$_3$CCH$_3$)(COCH$_3$)(I)] acyl product with the COCH$_3$ moiety in the apical position. The strong electron donation of the P(OCH$_2$)$_3$CCH$_3$ ligand accelerates the oxidation addition step of methyl iodide to [Rh(PhCOCHCOPh)(CO)(P(OCH$_2$)$_3$CCH$_3$)] by *ca.* 265 times faster (at 35°C) than that of the Monsanto catalyst, but inhibits the CO insertion step.

Keywords: *Benzoylacetone • Rhodium • Oxidative addition • Phosphite • DFT*

1. Introduction

Substitution and oxidative addition reactions of square planar d^8 electron rhodium(I) complexes are of particular importance for stoichiometric and catalytic reactions of coordination compounds [1]. An important example of a catalytic oxidative addition reaction is the reaction between methyl iodide and *cis*-[Rh(CO)$_2$I$_2$]$^-$. The first oxidative addition reaction is the rate-determining step in the rhodium based Monsanto carbonylation of methanol to acetic acid [2-4]. The electronic structure and reactivity of rhodium(I) complexes can be modified by the selection of the appropriate σ and π donor-acceptor ligands. Rhodium(I) complexes with β-diketones and triphenylphosphine or triphenylphosphite are of importance because of their catalytic activity in the hydroformylation of olefins [5-10].

The oxidative addition of iodomethane to bisphosphite complexes of the type [Rh(β-diketonato)(P(OPh)$_3$)$_2$] corresponds to a two step S$_N$2 mechanism via a five-coordinated transition state resulting in a trans-rhodium(III)-alkyl product [11-13]. The oxidative addition reaction of iodomethane with monophosphine complexes of the type [Rh(β-diketonato)(CO)(PPh$_3$)] is complicated by alkyl-acyl conversion reactions [14-21]. Characterization of the final products (alkyl *vs* acyl) and an understanding of the factors influencing these conversion reactions, are thus of primary importance. Understand the mechanism of activity of a catalyst requires an understanding of its structure in all the reaction steps. A combined experimental and computational chemistry study of the oxidative addition reaction of iodomethane with the monophosphite complex [Rh(PhCOCHCOPh)(CO)(P(OCH$_2$)$_3$CCH$_3$)], PhCOCH$_2$COPh = 1-phenyl-1,3-butanedione or benzoylacetone is discussed to provide a clear indication of the catalyst intervention.

2. Experimental procedure

2.1. Materials and apparatus

Solid reagents used in preparations (Merck, Aldrich and Fluka) were applied without further purification. Liquid reactants and solvents were distilled prior to use; water

* *E-mail: conradj@ufs.ac.za*

was doubly distilled. Organic solvents were dried according to published methods [40].

2.2. Synthesis

[Rh(PhCOCHCOPh)(CO)(P(OCH$_2$)$_3$CCH$_3$)] was prepared as described previously [31]. Characterization data. **IR** (KBr): v/cm^{-1}: 1992 (C=O). ^{1}H NMR (δ/ppm, acetone-d): 0.935 (s, 3H, phosphite-CH$_3$); 4.47 (d, 6H, 3 x OCH$_2$); 7.105 (s, 1H, CH), 7.43-7.57 and 8.07-8.14 (2xm, 10 H, phenyl). **^{31}P NMR** ((δ/ppm, acetone-d): 114.513 (d, 1P, phosphite-P, $^1J_{Rh-P}$ = 282.029 Hz).

2.3. Spectroscopy and spectrophotometry

NMR measurements at 298 K were recorded on a Bruker Avance DPX 300 NMR spectrometer (^{1}H 300.130 MHz). The chemical shifts were reported relative to SiMe$_4$ (0.00 ppm). Positive values indicated a downfield shift. Infrared spectra were recorded on a Hitachi 270-50 infrared spectrometer either in a KBr matrix or in chloroform solutions. UV measurements were recorded on a GBC-916 UV/VIS spectrophotometer equipped with a multi-cell thermostated cell holder (± 0.1°C).

2.4. Kinetic measurements

Oxidative addition reactions were monitored on the IR (by monitoring the formation and disappearance of the carbonyl peaks in chloroform) and on the UV/vis (by monitoring the change in absorbance at 410 nm in chloroform and acetone) spectrophotometers. All kinetic measurements were monitored under pseudofirst-order conditions with [CH$_3$I] in a 60 to 1000 times access over the concentration of the [Rh(PhCOCHCOPh)(CO)(P(OCH$_2$)$_3$CCH$_3$)] complex. The concentration [Rh(PhCOCHCOPh)(CO)(P(OCH$_2$)$_3$CCH$_3$)] ≅ 0.0002 mol dm^{-3} for UV/vis measurements and ≅ 0.003 mol dm^{-3} for IR measurements. Kinetic measurements, under pseudofirst-order conditions for different concentrations of [Rh(PhCOCHCOPh)(CO)(P(OCH$_2$)$_3$CCH$_3$)] at a constant [CH$_3$I], confirmed that the concentration of [Rh(PhCOCHCOPh)(CO)(P(OCH$_2$)$_3$CCH$_3$)] did not influence the observed kinetic rate constant. The observed first-order rate constants were obtained from least-square fits of absorbance *vs* time data [41]. The [Rh(PhCOCHCOPh)(CO)(P(OCH$_2$)$_3$CCH$_3$)] complex was tested for stability in solution by means of an overlay of IR and UV/vis spectra for at least 24 hours.

2.5. Calculations

Pseudofirst-order rate constants, k_{obs}, were calculated by fitting [41] kinetic data to the first-order equation [42]

$$A_t - A_\infty = (A_0 - A_\infty)\, e^{(-k_{obs} \times t)}$$

with A_t , A_∞ and A_0 = the absorbance of the indicated species at time t, infinity and 0 respectively. The experimentally determined pseudo first-order rate constants were converted to second- order rate constants, k_1, by determining the slope of the linear plots of k_{obs} against the concentration of the incoming iodomethane ligand. Non-zero intercepts implied that

$$k_{obs} = k_1[CH_3I] + k_{-1}.$$

All kinetic mathematical fits were completed utilizing the fitting program MINSQ [41]. The error of all the data was indicated according to crystallographic conventions, for example k_{obs} = 0.0236(1) s^{-1} implies k_{obs} = (0.0236 ± 0.0001) s^{-1}.

The activation parameters were determined by a least square fit to the Eyring equation [42]

$$k_2 = \frac{Tk_B}{h}\exp\left(-\frac{\Delta H^\#}{RT} + \frac{\Delta S^\#}{R}\right) \quad (2)$$

as well as from two linear forms of the equation [43]

$$\ln\frac{k_2}{T} = -\frac{\Delta H^\#}{RT} + \frac{\Delta S^\#}{R} + \ln\frac{k_B}{h} \quad (3)$$

and

$$T \text{ x } \ln\frac{k_2}{T} = T \text{ x } \left(\ln\frac{k_B}{h} + \frac{\Delta S^\#}{R}\right) - \frac{\Delta H^\#}{R} \quad (4)$$

with $\Delta H^\#$ = activation enthalpy, $\Delta S^\#$ = activation entropy, k_2 = second-order rate constant, k_B = Boltzmann's constant, T = temperature, h = Planck's constant, R = universal gas constant. Values determined for $\Delta H^\#$ and $\Delta S^\#$ using equations (2) to (4) were the same (see Fig. 3 and Fig. 4). The calculated standard errors obtained of $\Delta H^\#$ and $\Delta S^\#$ relate to the average experimental temperature [42,44]] within 8 K:

$$\frac{\sigma(\Delta H^\#)}{\sigma(\Delta S^\#)} = T_{av} \quad (5)$$

The activation Gibbs energy was calculated from equation [42]

$$\Delta G^\# = \Delta H^\# - T\Delta S^\# \quad (6)$$

2.6. Computational chemistry

Density functional theory (DFT) calculations were carried out using the ADF (Amsterdam Density Functional) 2009 programme [45-47] with the GGA (Generalized Gradient Approximation) functional PW91 (Perdew-Wang, 1991) [48]. The TZP (Triple ζ polarised) basis set with a fine mesh for numerical integration, a spin-restricted

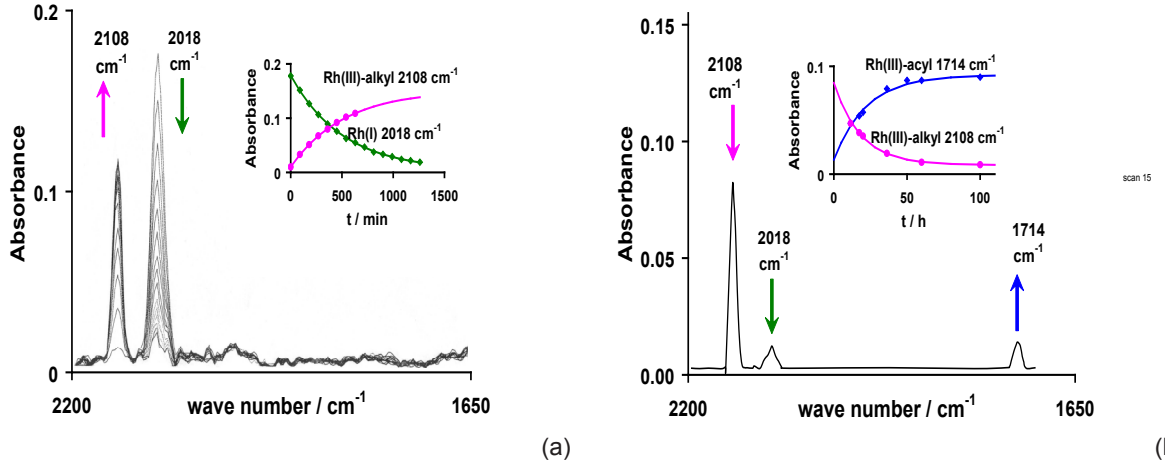

(a) (b)

Figure 1. Illustration of the oxidative addition reaction between CH_3I and [Rh(PhCOCHCOPh)(CO)(P(OCH$_2$)$_3$CCH$_3$)] as monitored on the IR spectrophotometer between 1650 – 2200 cm^{-1} in chloroform at 25ºC. (a) The first reaction (left, 90 s intervals) is indicated by the disappearance of Rh^{I} (peak at 2018 cm^{-1}) and the simultaneous appearance of Rh^{III}-alkyl (peak at 2108 cm^{-1}) at the same rate. (b) The second reaction is indicated by the simultaneous disappearance of Rh^{III}-alkyl (peak at 2108 cm^{-1}) and the formation of an Rh^{III}-acyl (peak at 1714 cm^{-1}) species. The inserts give the absorbance vs. time data of the indicated species. [CH_3I] = 0.1954 mol dm^{-3}, [Rh] = 2.6×10^{-3} mol dm^{-3}.

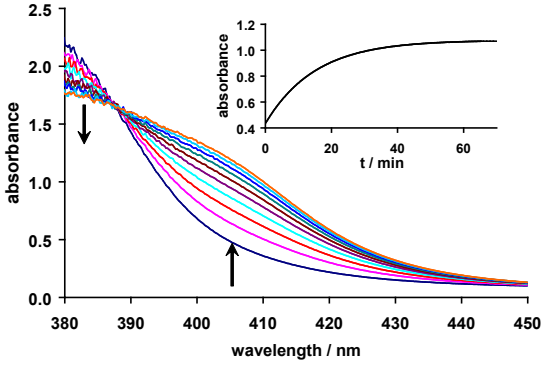

Figure 2. Selected repetitive UV/vis scans for the oxidative addition of CH_3I to [Rh(PhCOCHCOP)(CO)(P(OCH$_2$)$_3$CCH$_3$)] in chloroform at 25.0(1)°C. Inset Absorbance-time data collected at 410 nm. [CH_3I] = 0.1040 mol dm^{-3}, [Rh] = 2.5×10^{-4} mol dm^{-3}, k_{obs} = 0.0011092(3) s^{-1}.

formalism and full geometry optimization with tight convergence criteria, was used for minimum energy and transition state (TS) searches. Approximate structures of the TS have been determined with linear transit (LT) scans, with a constrained optimization along a chosen reaction coordinate, to sketch an approximate path over the TS between reactants and products. Numerical frequency analyses [49,50] where the frequencies are computed numerically by the differentiation of energy gradients in slightly displaced geometries, have been performed to verify the TS geometries. A TS has one imaginary frequency. Finally, the TS was allowed to relax after displacing the atoms according to the reaction coordinate as determined by the eigenvectors. Relaxing the TS from the minimum stretch of frequency gave the reactants (rhodium(I) and CH_3I). Relaxing the TS from the maximum stretch of frequency gave the products (the cationic five coordinated complex and I^-). Throughout, all calculations have been performed with no symmetry constraint (C_1), and all structures have been calculated as singlet states.

Zero point energy and thermal corrections (vibrational, rotational and translational) were made in the calculation of the thermodynamic parameters. The enthalpy (H) and Gibbs energy (G) were calculated from [42]

$$U = E_{TBE} + E_{ZPE} + E_{IE}$$

$$H = U + RT \text{ (gas phase) or } H = U \text{ (solution)}$$

$$G = H - TS$$

where U is the total energy, E_{TBE} is the total bonding energy, E_{ZPE} is the zero point energy, E_{IE} is the internal energy (sum of vibrational, rotational and translational energies), R is the gas constant, T is the temperature and S is the entropy. The entropy (S) was calculated from the temperature dependent partition function in ADF at 298.15 K. The computed results assumed an ideal gas.

Solvent effects were taken into account for all reported calculations. The COSMO (Conductor like Screening Model) model of solvation [51-53] was used as implemented [54] in ADF. The COSMO model

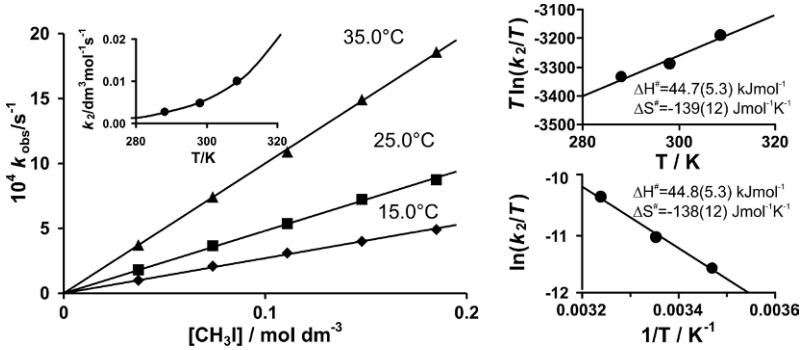

Figure 3. Temperature and iodomethane concentration dependence for observed pseudofirst-order rate constants k_{obs} for the oxidative addition of iodomethane to [Rh(PhCOCHCOPh)(CO)(P(OCH$_2$)$_3$CCH$_3$)] in acetone at 410 nm, [Rh] = 2.5×10^{-4} mol dm^{-3}. Inset: Eyring plot according to Eq. 2. Right: Eyring plots according to Eqs. 3 and 4.

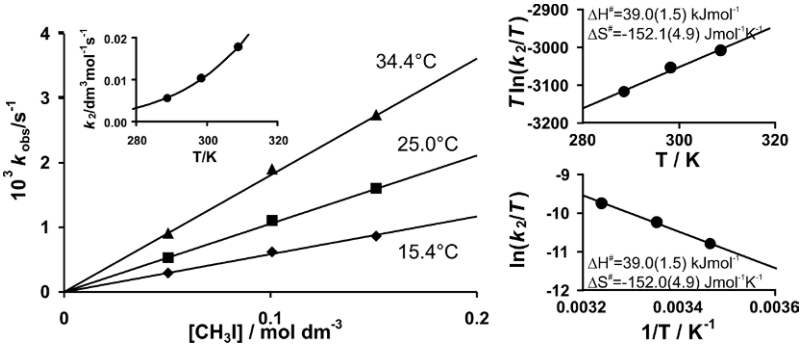

Figure 4. Temperature and iodomethane concentration dependence for observed pseudofirst-order rate constants k_{obs} for the oxidative addition of iodomethane to [Rh(PhCOCHCOPh)(CO)(P(OCH$_2$)$_3$CCH$_3$)] in $CHCl_3$ at 410 nm, [Rh] = 2.5×10^{-4} mol dm^{-3}. Inset: Eyring plot according to Eq. 2. Right: Eyring plots according to Eqs. 3 and 4.

is a dielectric model in which the solute molecule is embedded in a molecule-shaped cavity surrounded by a dielectric medium with a given dielectric constant (ε_0). The type of cavity used is Esurf [55] and the solvent used is methanol (ε_0 = 32.6). The activation parameters were also calculated in chloroform (ε_0 = 4.8) and acetone (ε_0 = 20.7) as solvents.

3. Results and discussion

3.1. Synthesis and identification of complexes

In dicarbonyl [Rh(β-diketonato)(CO)$_2$] complexes, only one CO group is exchanged for PPh_3 even with the addition of an excess PPh_3 [22]. In contrast, the main product of the reaction between [Rh(β-diketonato)(CO)$_2$] and an excess of triphenylphosphite ($P(OPh)_3$) is [Rh(β-diketonato)(P(OPh)$_3$)$_2$]. Only with less than 2 moles of $P(OPh)_3$, [Rh(β-diketonato)(CO)(P(OPh)$_3$)] was produced [23]. Strong π-acceptors such as PR_3 = $P(OPh)_3$ are necessary to obtain di-substituted [Rh(β-diketonato)(PR$_3$)$_2$]. With weak π-acceptors, such as PPh_3, even when they are used in a large excess, only the monosubstituted product is obtained [24]. The bicyclic phosphite 4-methyl-2,6,7-trioxa-1-phosphabicyclo[2.2.2] octane ligand with a Tolman electronic parameter [25] of ν(CO) = 2087.3 cm^{-1} similar to that of $P(OPh)_3$ (2085.3 cm^{-1}) is expected to exhibit a strong π-accepting ability [26]. However, even with an excess of $P(OCH_2)_3CCH_3$ added to [Rh(PhCOCHCOPh)(CO)$_2$], only the mono substituted [Rh(PhCOCHCOPh)(CO)(P(OCH$_2$)$_3$CCH$_3$)] complex was obtained. Back donation to the phosphite ligand tends to reduce electron density on the central metal atom to a larger extent compared to PPh_3. This leads to a weakened ability to reduce the CO bond order in the title compound. This is demonstrated by comparing the carbonyl stretching frequency of the title compound [Rh(PhCOCHCOPh)(CO)(P(OCH$_2$)$_3$CCH$_3$)] (ν(CO) = 1992 cm^{-1} (KBr), 2018 cm^{-1} (CH_3Cl solution)) with that of the tri-phenylphosphine analogue [Rh(PhCOCHCOPh)(CO)(PPh_3)] (ν(CO) = 1972 and 1982 cm^{-1} representing the two molecules in the asymmetric unit) [27].

3.2. Kinetics

3.2.1. Infrared study

Infrared spectroscopy is ideal to distinguish between complexes containing CO bonds in metal-CO complexes

of Rh^{I}-carbonyl complexes or Rh^{III}-carbonyl complexes and CO bonds in metal-COCH$_3$ complexes of Rh^{III}-acyl complexes. CO bonds in Rh^{I}-monocarbonylphosphine complexes resonate at ~1980 – 2050 cm^{-1} and at ~2050 – 2150 cm^{-1} for Rh^{III}-alkyl complexes. CO bonds in Rh^{III}-acyl complexes resonate at ~ 1700 – 1750 cm^{-1} [28,29]. The reaction progress between CH_3I and [Rh(PhCOCHCOPh)(CO)(P(OCH$_2$)$_3$CCH$_3$)] in $CHCl_3$ was firstly followed using IR spectroscopy by monitoring the changes in absorbance of peaks at different ν(CO) bands in the range of 1650 - 2200 cm^{-1}. A typical series of the spectra of the oxidative addition reaction of CH_3I to [Rh(PhCOCHCOPh)(CO)(P(OCH$_2$)$_3$CCH$_3$)] as well as the subsequent carbonyl insertion step, is shown in Fig. 1. The *first* reaction step shows that the disappearance of the Rh^{I}-CO complex (at 2018 cm^{-1}, k_{obs} = 1.98(3)×10^{-3} s^{-1}) basically corresponds to the formation of the Rh^{III}-CO complex (at 2108 cm^{-1}, k_{obs} = 1.92(8)×10^{-3} s^{-1} for [CH_3I] = 0.1954 mol dm^{-3}). The band at 2108 cm^{-1} is assigned to a Rh^{III}-alkyl product [Rh(PhCOCHCOPh)(CO)(P(OCH$_2$)$_3$CCH$_3$)(CH$_3$)(I)]. The half-life of this reaction is 350 s and this reaction goes to completion, *i.e.* all Rh(I) are converted to the first Rh^{III}-alkyl product. This *first* reaction step is followed by a much slower reaction ($t_{1/2}$ ≈ 13 hours, Fig. 1b). This step involves the formation of the Rh^{III}-COCH$_3$ species (at 1714 cm^{-1}, k_{obs} = 1.25(9)×10^{-5} s^{-1}) corresponding to the depletion of the Rh^{III}-CO (alkyl) signal (at 2108 cm^{-1}, k_{obs} = 1.52(6)×10^{-5} s^{-1}). The Rh^{III}-acyl results from the migratory insertion of the methyl group of the Rh^{III}-alkyl to the carbonyl group. Since the *second reaction* is *ca*. 130 times slower than the *first reaction*, it was treated in isolation. Data from the interface at the boundary between the two reactions were, however, disregarded. This *second reaction* was found to be independent of [CH_3I]. The kinetic data of the *first* and *second* reaction steps are consistent with

$$Rh^{I} + CH_3I \underset{k_{-1}}{\overset{k_1}{\rightleftharpoons}} Rh^{III}\text{-alkyl} \underset{(k_{-2})}{\overset{k_2}{\rightleftharpoons}} Rh^{III}\text{-acyl}$$

with $k_{-1} \approx 0 \approx k_{-2}$.

3.2.2. UV/vis, solvent and temperature dependence study

When following the reaction between CH_3I and [Rh(PhCOCHCOPh)(CO)(P(OCH$_2$)$_3$CCH$_3$)] in $CHCl_3$ on an UV/vis spectrophotometer, two reaction steps could be identified. Fig. 2 shows repetitive UV/vis scans for the first step of the oxidative addition reaction of CH_3I to [Rh(PhCOCHCOPh)(CO)(P(OCH$_2$)$_3$CCH$_3$)] in chloroform. The single isosbestic point at 387 nm, indicate the absence of the insertion step (k_2-step) on the investigated time scale. The change in absorbance was monitored at 410 nm (see inset in Fig. 2). The reaction rate constant obtained for the first step corresponds to the rate constant for the disappearance of the Rh^{I} monocarbonyl species as observed by IR. The rate constant for the second step

Table 1. Kinetic rate constants and activation parameters for the oxidative addition of iodomethane to [Rh(PhCOCHCOPh)(CO)(P(OCH$_2$)$_3$CCH$_3$)] in various solvents, as monitored by IR and UV/vis spectrophotometry at the indicated temperatures. k_1 (second order) and k_2 (first order) are the rate constants associated with the first and second stages of the reaction of CH_3I to [Rh(PhCOCHCOPh)(CO)(P(OCH$_2$)$_3$CCH$_3$)]. The DFT calculated activation parameters are also given in selected solvents. Data for [Rh(CH$_3$COCHCOCH$_3$)(CO)(P(OCH$_2$)$_3$CCH$_3$)] and the Monsanto catalyst are included for comparative purposes.

Method	Solvent	ε	Oxidative addition reaction						CO insertion
			$10^3 k_1$ / dm^3 mol^{-1} s^{-1}			$\Delta H^{\#}$ / kJ mol^{-1}	$\Delta S^{\#}$ / JK^{-1} mol^{-1}	$\Delta G^{\#}$ / kJ mol^{-1}	k_2 / s^{-1}
			15°C	25°C	35°C				
			[Rh(PhCOCHCOPh)(CO)(P(OCH$_2$)$_3$CCH$_3$)]						
IR	Chloroform	4.8		10.12(2)					0.0000152(8)
UV/vis	Chloroform	4.8	5.85(5)	10.57(9)	18.07(10)	39.0(1.5)	-152.0(4.9)	84	
	Acetone	20.7	2.70(7)	4.81(9)	10.00(9)	44.8(5.3)	-138(12)	86	
DFT	Acetone	20.7				24	-192	82	
	Chloroform	4.8				29	-170	80	
	Methanol	32.6				24	-194	82	
			[Rh(CH$_3$COCHCOCH$_3$)(CO)(P(OCH$_2$)$_3$CCH$_3$)] [a]						
IR	Chloroform	4.8		17.5(3)					0.0000127(8)
UV/vis	Benzene	2.3	0.28(1)	0.45(2)	0.89(4)	42(4)	-168(15)	92	
	Chloroform	4.8	9.44(5)	17.34(4)	29.93(8)	40.5(8)	-143(3)	83	0.0000119(1)
	Acetone	20.7	3.36(3)	5.54(7)	10.18(9)	43(3)	-145(9)	86	
	Methanol	32.6	17.9(3)	36.0(5)		64(3)	-56(11)	81	
DFT	Methanol	32.6				26	-160	73	
			Monsanto catalyst [b]						
IR	CH_2Cl_2			0.068				100	0.13

[a] *From [30]*
[b] *From [56]*

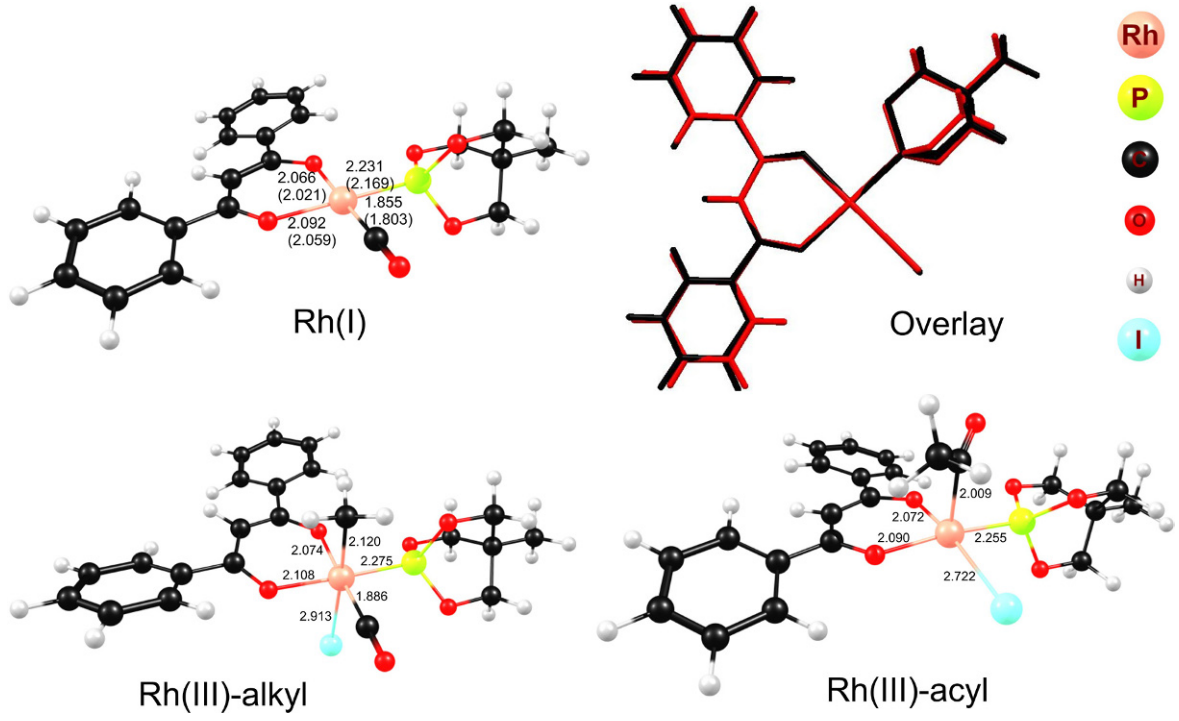

Figure 5. DFT optimized structure of the reactant [Rh(PhCOCHCOPh)(CO)(P(OCH$_2$)$_3$CCH$_3$)], the overlay of calculated (black) and experimental (red) [Rh(PhCOCHCOPh)(CO)(P(OCH$_2$)$_3$CCH$_3$)] and the lowest energy [Rh(PhCOCHCOPh)(CO)(P(OCH$_2$)$_3$CCH$_3$)(CH$_3$)(I)]-alkyl and [Rh(PhCOCHCOPh)(P(OCH$_2$)$_3$CCH$_3$)(COCH$_3$)(I)]-acyl reaction products. Distances (Å, black) and colour code (online version) of the atoms are as indicated. Experimental bond lengths are in brackets.

(not shown in Fig. 2) corresponds to the rate constant for the formation of the Rh^{III}-acyl species, which is the *second reaction* as observed on the IR spectrophotometer.

Plots of k_{obs} *vs*. [CH$_3$I] for the *first reaction* in chloroform and in acetone are linear with a zero intercept (Fig. 3 and Fig. 4), indicating the reaction to be first order in CH$_3$I and hence second order overall. This result is consistent with the rate law:

$$k_{obs} = k_1[CH_3I]$$

with k_1 as the second order rate constant. As was expected, the observed rate constant for the *second* insertion reaction was independent of [CH$_3$I] in the range $0 < [CH_3I] < 0.2$ mol dm^{-3}. Values of k_1 obtained from the slopes of the k_{obs} *vs* [CH$_3$I] plots, are summarized in Table 1. The activation parameters ($\Delta H^{\#}$, $\Delta S^{\#}$) were determined in both solvents to investigate the character of the transition state. Fig. 3 and Fig. 4 display the different Eyring plots, and Table 1 gives a summary of the activation parameters. The relatively small $\Delta H^{\#}$ values, accompanied by large negative $\Delta S^{\#}$ values, indicate an associative mechanism including bond formation and/or partial charge creation (electrostriction) during the formation of the transition state. A high pressure kinetic study of the oxidative addition of

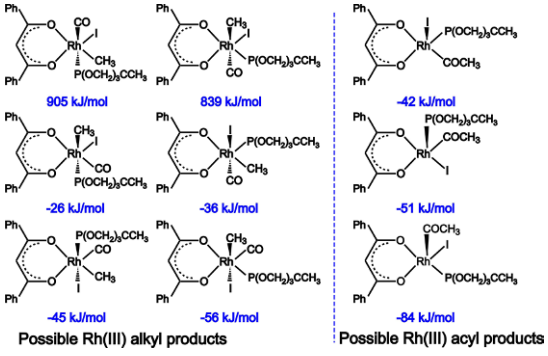

Figure 6. Geometries and ADF calculated relative energies (ΔE_{TBE}) of the possible rhodium(III) alkyl and acyl products of the [Rh(PhCOCHCOPh)(CO)(P(OCH$_2$)$_3$CCH$_3$)] + CH$_3$I reaction. The energy of the reactants is taken as zero.

CH$_3$I to [Rh(CH$_3$COCHCOCH$_3$)(CO)(P(OCH$_2$)$_3$CCH$_3$)] yields an experimental volume of activation, $\Delta V^{\#}$ of -28(1) cm^3 mol^{-1} in the relative polar solvent acetone [30]. This result could allow charge creation in the transition state, favouring the formation of an ion-pair intermediate, which suggested that the oxidative addition of iodomethane to [Rh(CH$_3$COCHCOCH$_3$)(CO)(P(OCH$_2$)$_3$CCH$_3$)] most probably proceeds *via* the linear transition state. An intimate two step S$_N$2 mechanism similar to that presented by Swaddle and co-workers [11] for the oxidative addition of iodomethane to β-diket

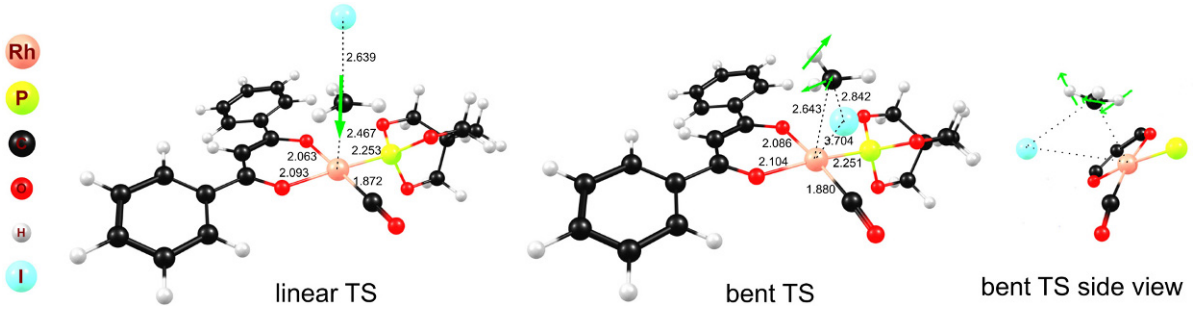

Figure 7. DFT optimized structure of the "linear/back" and "bent" transition states of the reaction [Rh(PhCOCHCOPh)(CO)(P(OCH$_2$)$_3$CCH$_3$)] + CH$_3$I. The Gibbs energies ($\Delta G^{\neq}$) of the transition states are 82 and 196 kJ mol^{-1} (0.85 and 2.03 eV) respectively, calculated in methanol as solvent. The displacement vectors (green arrows) indicate the movement of the CH$_3^+$ group at the negative frequency (-235.0 cm^{-1} with a calculated intensity of -481 for the linear TS and -319.0 cm^{-1} with a calculated intensity of -239 for the bent TS). Distances (Å, black) and colour code (online version) of the atoms are as indicated.

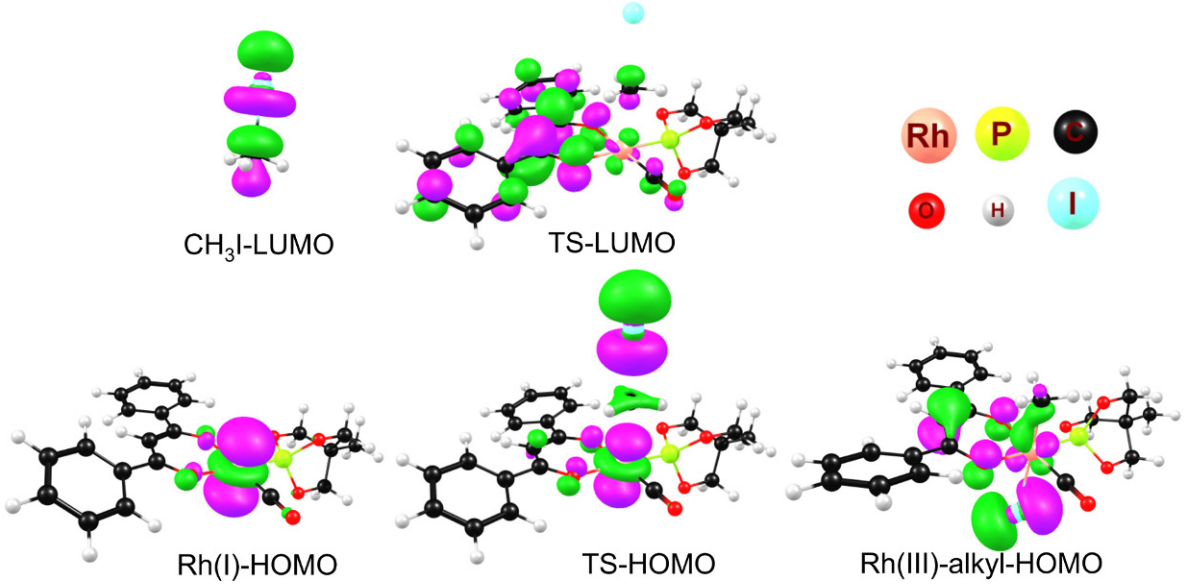

Figure 8. Visualization of selected molecular orbitals of the reactants, transition state (TS) and the Rhodium(III)-alkyl reaction product of the oxidative addition reaction [Rh(PhCOCHCOPh)(CO)(P(OCH$_2$)$_3$CCH$_3$)] + CH$_3$I. Note the d_{z2}-orbital at the rhodium centre of the TS HOMO diagram and the p_z-orbital at the methyl group of the TS LUMO diagram. The colour code (online version) of the atoms is as indicated.

onatobis(triphenylphosphite) complexes of Rh(I) is thus proposed for the oxidative addition step of iodomethane to [Rh(PhCOCHCOPh)(CO)(P(OCH$_2$)$_3$CCH$_3$)].

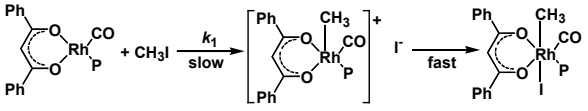

The proposed first step may be represented as:

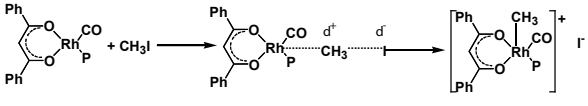

The resulting *trans*-adduct can easily undergo an acyl formation reaction (CH$_3$ and CO located *cis* to each other). Density functional theory results of this study also showed *trans* addition of methyliodide to [Rh(PhCOCHCOPh)(CO)(P(OCH$_2$)$_3$CCH$_3$)] *via* a linear transition state, see paragraph 2.2.3 below.

3.2.3. Computational study

To gain more insight into the geometry of the reactants, the transition state and reaction products of the [Rh(PhCOCHCOPh)(CO)(P(OCH$_2$)$_3$CCH$_3$)] + CH$_3$I oxidative addition reaction, results of a density functional theory (DFT) study are presented. The DFT optimized geometry of [Rh(PhCOCHCOPh)(CO)(P(OCH$_2$)$_3$CCH$_3$)] is given in Fig. 5. The geometry of [Rh(PhCOCHCOPh)(CO)(P(OCH$_2$)$_3$CCH$_3$)] is square planar, with bond lengths and angles similar to that found for the crystal structure of [Rh(PhCOCHCOPh)(CO)(P(OCH$_2$)$_3$CCH$_3$)] [31] (see Fig. 5) for an overlay of the experimental and calculated structure of [Rh(PhCOCHCOPh)(CO)

($P(OCH_2)_3CCH_3$)]). Oxidative addition of iodomethane to [Rh(PhCOCHCOPh)(CO)($P(OCH_2)_3CCH_3$)] leads to a rhodium(III) alkyl product. Six possible rhodium(III) oxidative addition product isomers of the formula [Rh(PhCOCHCOPh)(CO)($P(OCH_2)_3CCH_3$)(CH_3)(I)] are possible (Fig. 6). One isomer results from the *trans* addition of iodomethane and five isomers result from the *cis* addition or from the re-arrangement of a *trans* addition product. The calculated relative electronic energies of the optimized geometries of the six possible rhodium(III) oxidative addition product isomers of the formula [Rh(PhCOCHCOPh)(CO)($P(OCH_2)_3CCH_3$)(CH_3)(I)] are also displayed in Fig. 6. These energies indicate that the *trans* alkyl product isomer is the most stable product of oxidative addition of iodomethane to [Rh(PhCOCHCOPh)(CO)($P(OCH_2)_3CCH_3$)]. DFT calculations on the structurally similar rhodium-β-diketonato complexes, [Rh(β-diketonato)(CO)(PPh_3)] with β-diketone = 4,4,4-trifluoro-1-(2-thenoyl)-1,3-propanedione, 1-phenyl-3-(2-thenoyl)-1,3-propanedione, 1,3-di(2-thenoyl)-1,3-propanedione [32] 1-ferrocenyl-4,4,4-trifluorobutane-1,3-dione [33] or acetylacetone [34], in agreement with experimental observations [17,18], also indicate the *trans* addition of CH_3I to the square planar rhodium(I) complexes. The *trans* addition of iodomethane to the bisphosphite complex [Rh($CH_3COCHCOCH_3$)($P(OPh)_3$)$_2$], in agreement with ^{1}H NMR data [11], was confirmed by a density functional theory (DFT) computational study of the transition state and product of the oxidative addition reaction [12].

Two types of transition state structures ("linear/back" and "bent") leading to *trans* addition products have been reported on the oxidative addition of methyl iodide to square planar Rh(I) complexes [35,36]. Fig. 7 shows the optimized geometries of the linear/back and the bent transition states calculated for the [Rh(PhCOCHCOPh)(CO)($P(OCH_2)_3CCH_3$)] + CH_3I reaction of this study. The linear/back transition state structure corresponds to an S_N2 mechanism, characterized by a linear Rh-C_{CH3}-I arrangement and by a Rh-C_{CH3}-H angle close to 90°. The methyl hydrogen atoms are located in the equatorial plane of the five-coordinated carbon atom, resulting in a trigonal bipyramidal arrangement. The bent transition state structure corresponds to a side-on approach of the C_{CH3}-I bond to the rhodium atom, leading to the same intermediate product as the linear/back transition state structure - a cationic five-coordinated rhodium complex and a free iodide ion. The linear/back transition state is favoured by 114 kJ mol^{-1} over the bent transition state, calculated in methanol as a solvent. The geometry of the *trans* rhodium(III) alkyl oxidative addition product is displayed in Fig. 5.

The displacement vectors of the imaginary frequency of the transition state structure are shown in Fig. 7. The negative frequency of -235.0 cm^{-1} with a calculated intensity of -481 for the linear transition state corresponds to a CH_3I stretching vibrational mode in which the I-C_{CH3} bond breaks and the Rh-C_{CH3} bond forms. The transition state displacement vectors of the bent transition state (-319.0 cm^{-1} with a calculated intensity of -239) can be described as Rh-C_{CH3}-I bending in which the CH_3^+ group is making a rocking movement between Rh and I (See Fig. 7 right).

Fig. 8 displays selected molecular orbitals of the reactants, the transition state and the *trans* rhodium(III) alkyl oxidative addition product. The Rh(I) reactant is a $d_{xz}^2\ d_{yz}^2\ d_{xy}^2\ d_{z2}^2\ d_{x2-y2}^0$ complex of which the HOMO (highest occupied molecular orbital) exhibits mainly a d_{z2} character. The LUMO (lowest unoccupied molecular orbital) of free CH_3I has p_z character on the methyl carbon. The calculated C_{CH3}-I bond length in the free methyl iodide is 2.18 Å. This C_{CH3}-I bond length increases to 2.64 Å in the transition state (Fig. 7). At this point, the CH_3 group is 2.47 Å away from the rhodium centre, and the methyl hydrogen atoms are located in an equatorial plane with a Rh-C_{CH3}-H angle close to 90°. The main contribution to the Rh-C_{CH3} bond in the transition state comes from the overlap of the d_{z2} HOMO of the rhodium atom with the p_z LUMO of the methyl carbon (Fig. 8). The CH_3 group continues to move closer to the rhodium centre. Following the TS, is the formation of the cationic five-coordinate [Rh(PhCOCHCOPh)(CO)($P(OCH_2)_3CCH_3$)(CH_3)]$^+$ intermediate with the CH_3 group in the apical position and with the iodide ion drifting away into the solvent sphere. The relative energy of the intermediate is 14 kJ mol^{-1} less than that of the transition state. A free iodide coordinates to the rhodium centre to form the *trans* rhodium(III) alkyl oxidative addition product with a final Rh-I bond length of 2.91 Å and energy of 57 kJ mol^{-1} lower than the intermediate. An inversion of the configuration at the methyl carbon occurred, and the methyl group was fully bonded to the rhodium atom through a p_z-d_{xz} interaction in the HOMO (Fig. 8).

The calculated activation parameters for the oxidative addition step are summarized in Table 1. The calculated activation Gibbs energy of the transition state (82 kJ mol^{-1} in acetone as solvent) leading to *trans* rhodium(III) alkyl is in acceptable agreement with the experimental value of 86 kJ mol^{-1} in acetone as a solvent. The agreement between experiment and theory for the individual components $\Delta H^{\neq}$ and $\Delta S^{\neq}$ to $\Delta G^{\neq} = H^{\neq} - T\Delta S^{\neq}$ is not as good as for $\Delta G^{\neq}$ itself. The large compensating variations $\Delta H^{\neq}$ and $\Delta S^{\neq}$ with a modest change in $\Delta G^{\neq}$ were also found by Ziegler [37].

CO insertion in a rhodium(III) alkyl product leads to a rhodium(III) acyl product. The most stable geometry calculated for the various possible [Rh(PhCOCHCOPh)(P(OCH$_2$)$_3$CCH$_3$)(COCH$_3$)(I)] acyl products (Fig. 6) is square pyramidal with the COCH$_3$ moiety in the apical position (See Fig. 5 for the optimized geometry). Trigonal-bipyramidal geometries were too high in energy to be considered. All crystal structures of five-coordinated square pyramidal rhodium(III) acyl complexes, have the COCH$_3$ moiety in the apical position [38]. The structurally similar [Rh((cupf)(P(OCH$_2$)$_3$CCH$_3$)(COCH$_3$)(I)] acyl (Hcupf = N-hydroxy-N-nitroso-benzeneamine or cupferron) also adopts a square pyramidal geometry with the COCH$_3$ moiety in the apical position [39]. Therefore, both computational calculations and crystallographic data are consistent with the geometry of the thermodynamic stable reaction product to be square-pyramidal with the COCH$_3$ group in the apical position. However, it is not possible to determine if the observed acyl product is the final reaction product or only a reaction intermediate leading to the most stable acyl product.

3.2.4. Mechanistic and Reactivity correlation: Methyl Iodide to [Rh(RCOCHCOR)(CO)(P(OCH$_2$)$_3$CCH$_3$)] (R = CH$_3$ or Ph) and the Monsanto catalyst

The rate-determining step in the rhodium-iodide catalyzed reaction of methanol to acetic acid is the oxidative addition of iodomethane to [Rh(CO)$_2$I$_2$]$^-$ to produce the [Rh(CH$_3$)(CO)$_2$I$_3$]$^-$ alkyl reaction intermediate that rapidly converts to an acyl [Rh(CH$_3$CO)(CO)I$_3$]$^-$. This reaction is similar to the reaction between [Rh(RCOCHCOR)(CO)(P(OCH$_2$)$_3$CCH$_3$)] and iodomethane (R = Ph in this study or R = CH$_3$ from [30]):

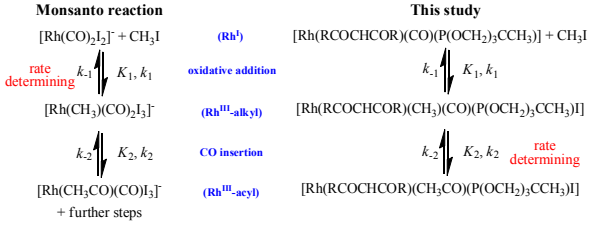

Rate constants for the above reactions are compared in Table 1. The second order rate constant for the oxidative addition reaction of this study (R = Ph) is slightly smaller than the rate constant measured for the corresponding reaction with R = CH$_3$: [Rh(CH$_3$COCHCOCH$_3$)(CO)(P(OCH$_2$)$_3$CCH$_3$)] + CH$_3$I. The rate constants for the CO insertion step, however, are kinetically indistinguishable. It is clear that the combination of the bidentate (RCOCHCOR)$^-$ ligand (with R = Ph or R = CH$_3$) and the phosphorus ligand leads to an increased reactivity of Rh^I with iodomethane if compared to the Monsanto catalyst. The oxidative addition step is accelerated but the CO insertion step is slowed down.

4. Conclusions

The reaction rate of the oxidative addition and CO insertion steps of methyl iodide with [Rh(PhCOCHCOPh)(CO)(P(OCH$_2$)$_3$CCH$_3$)] have been determined. Large negative experimental values for the activation entropy and results from a DFT computational chemistry study indicated *trans* addition of the CH$_3$I to [Rh(PhCOCHCOPh)(CO)(P(OCH$_2$)$_3$CCH$_3$)]. CO insertion leads to a square pyramidal [Rh(PhCOCHCOPh)(P(OCH$_2$)$_3$CCH$_3$)(COCH$_3$)(I)] acyl product with the COCH$_3$ moiety in the apical position. The strong electron donation of the P(OCH$_2$)$_3$CCH$_3$ ligand accelerates the oxidation addition step of methyl iodide to [Rh(PhCOCHCOPh)(CO)(P(OCH$_2$)$_3$CCH$_3$)] by *ca* 265 times (at 35°C) faster than the Monsanto catalyst, but inhibits the CO insertion step.

Acknowledgements

Financial assistance by the South African National Research Foundation and the Central Research Fund of the University of the Free State is gratefully acknowledged.

Supporting Information Available

Cartesian coordinates (in Å) of the structures associated with this study.

References

[1] J.P. Collman, L.S. Hegedus, J.R. Norton, R.G. Finke, Principles and Applications of Organotransition Metal Chemistry (University Science Books, California, 1987)
[2] A. Haynes, B.E. Mann, P.M. Maitlis, J. Am. Chem. Soc. 115, 4093 (1993)
[3] L. Cavallo, M. Sola, J. Am. Chem. Soc. 123, 12294 (2001)
[4] A. Haynes, P.M. Maitlis, G.E. Morris, G.J. Sunley, H. Adams, P.W. Badger, C.M. Bowers, D.B. Cook, P.I.P. Elliot, T. Ghaffer, H. Green, T.R. Griffin, M. Payne, J.M. Pearson, M.J. Taylor, P.W. Vickers, R. Watt, J. Am. Chem. Soc. 126, 2847 (2007)
[5] E. Mieczynska, A.M. Trzeciak, J.J. Ziólkowski, J. Mol.

Catal. 80, 189 (1993)
[6] A.M. Trzeciak, E. Mieczynska, J.J. Ziólkowski, Topics in Catalysis 11/12 461(2000)
[7] J.H. Subramaniam, B. Ghosh, A. Tunge, J. AIChE Journal 52, 2575 (2006)
[8] C.S. Vasem, S. Modem, S. Kankala, S. Kanne, G. Budige, R. Vadde, Cent. Eur. J. Chem. 8, 77 (2010)
[9] M. Haumann, R. Meijboom, J.R. Moss, A. Roodt, Dalton Trans. 1679 (2004)
[10] R. Crous, M. Datt, D. Foster, L. Bennie, C. Steenkamp, J. Huyser, L. Kirsten, G. Steyl, A. Roodt, Dalton Trans. 1108 (2005)
[11] G.J. Van Zyl, G.J. Lamprecht, J.G. Leipoldt, T.W. Swaddle, Inorg. Chim. Acta 143, 223 (1988)
[12] M.M. Conradie, J. Conradie, J. Organomet. Chem. 695, 2126 (2010)
[13] M.M. Conradie, J.J.C. Erasmus, J. Conradie, Polyhedron, 20, 2345 (2011)
[14] S.S. Basson, J.G. Leipoldt, J.T. Nel, Inorg. Chim. Acta 84, 167 (1998)
[15] J.G. Leipoldt, E.C. Steynberg, R. van Eldik, R. Inorg. Chem. 26, 3068 (1987)
[16] J. Conradie, G.J. Lamprecht, A. Roodt, J.C. Swarts, Polyhedron 23, 5075 (2007)
[17] M.M. Conradie, J. Conradie, Inorg. Chim. Acta. 361, 208 (2008)
[18] M.M. Conradie, J. Conradie, Inorg. Chim. Acta. 361, 2285 (2008)
[19] J. Conradie, J.C. Swarts, Organometallics, 28, 1018 (2009)
[20] A. Roodt, G. Visser, A. Brink, Crystallography Reviews 17, 241 (2011)
[21] A. Brink, A. Roodt, G. Steyl, H.G. Visser, Dalton Trans. 39, 5572 (2010)
[22] A.M. Trzeciak, J.J. Ziólkowski, Inorg. Chim. Acta 96, 15 (1985)
[23] E. van Eldik, S. Aygen, H. Kelm, A.M. Trzeciak, J.J. Ziólkowski, Transition Met. Chem. 10, 167 (1985)
[24] W. Simanko, K. Mereiter, R. Schmid, K. Kirchner, A.M. Trzeciak, J.J. Ziólkowski, J. Organomet. Chem. 602, 59 (2000)
[25] C.A. Tolman, W.C. Seidel, L.W. Gosser, J. Am. Chem. Soc. 96, 53 (1974)
[26] C.A. Tolman, Chem. Rev. 77, 313 (1977)
[27] D. Lamprecht, G. J. Lamprecht, J. M. Botha, K. Umakoshi, Y. Sasaki, Acta Cryst. C53, 1403 (1997)
[28] J. Conradie, G.J. Lamprecht, S. Otto, J.C. Swarts, Inorg. Chim. Acta 328, 191 (2002)
[29] N.F. Stuurman, J. Conradie, J. Organomet. Chem. 694, 259 (2009)
[30] J.J.C. Erasmus, J. Conradie, Inorg. Chim. Acta 375, 128 (2011)
[31] J.J.C. Erasmus, G.J. Lamprecht, T. Kohzuma, Y. Nakano Acta Cryst. C54, 1085 (1998)
[32] M.M. Conradie, J. Conradie, Inorg. Chim. Acta 362, 519 (2009)
[33] M.M. Conradie, J. Conradie, S. Afr. J. Chem. 61, 102 (2008)
[34] M.M. Conradie, J. Conradie, Dalton, 40, 8226 (2011)
[35] M. Feliz, Z. Freixa, P. W. N. M. van Leeuwen, C. Bo, Organometallics 24, 5718 (2005)
[36] T.R. Griffin, D.B. Cook, A. Haynes, J.M. Pearson, D. Monti, G.E. Morris, J. Am. Chem. Soc. 117, 3029 (1996)
[37] M. Cheong, T. Ziegler, Organometallics 24, 3053 (2005)
[38] Cambridge Structural Database (CSD), Version 5.32, November 2010 update (The Cambridge Crystallographic Data Centre, Cambridge, UK, 2010)
[39] J.A. Venter, W. Purcell, H.G. Visser, Acta Cryst E65, m1528 (2009)
[40] B.S. Furniss, A.J. Hannaford, P.W.G. Smith, A.R. Tatchell, Vogel's Textbook of Practical Organic Chemistry, 5th edition (John Wiley & Sons, New York, 1994) 409
[41] L. Helm, MINSQ, Non-Linear parameter estimation and model development, least squares parameter optimization V4.02 (MicroMath Inc, Salt Lake City, UT, 1991)
[42] J.H. Espenson, Chemical Kinetics and Reaction Mechanisms, 2nd edition (McGraw-Hill, New York, 1995) pp. 15, 49, 70-75, 156
[43] G. Lente, I. Fabian, A.J. Poe, New. J. Chem. 29, 759 (2005)
[44] R.C. Petersen, J.H. Markgraf, S.D. Ross, J. Am. Chem. Soc. 83, 3819 (1961)
[45] G. te Velde, F.M. Bickelhaupt, E.J. Baerends, C. Fonseca Guerra, S.J.A. van Gisbergen, J.G. Snijders, T. Ziegler, J. Comput. Chem. 22, 931 (2001)
[46] C. Fonseca Guerra, J.G. Snijders, G. te Velde, E.J. Baerends, Theor. Chem. Acc. 99, 391 (1998)
[47] ADF2009.01, SCM, Theoretical Chemistry (Vrije Universiteit, Amsterdam, The Netherlands, 2009)
[48] J.P. Perdew, J.A. Chevary, S.H. Vosko, K.A. Jackson, M.R. Pederson, D.J. Singh, C. Fiolhais, Phys. Rev. B 46, 6671 (1992); Erratum: J.P. Perdew, J.A. Chevary, S.H. Vosko, K.A. Jackson, M.R. Perderson, D.J. Singh, C. Fiolhais, Phys. Rev. B 48 4978 (1993)
[49] L. Fan, T. Ziegler, J. Chem. Phys. 96, 9005 (1992)

[50] L. Fan, T. Ziegler, J. Amer. Chem. Soc. 10890 (1992)
[51] A. Klamt, G. Schüürmann, J. Chem. Soc., Perkin Trans. 2, 799 (1993).
[52] A. Klamt, J. Phys. Chem. 99, 2224 (1995)
[53] A. Klamt, V. Jones, J. Chem. Phys. 105, 9972 (1996).
[54] C.C. Pye, T. Ziegler, Theor. Chem. Acc. 101, 396 (1999).
[55] J.L. Pascual-Ahuir, E. Silla, I. Tuñon, J. Comput. Chem. 15, 1127 (1994).
[56] P.M. Maitlis, A. Haynes, G.J. Sunley, M.J.J. Howard, Chem. Soc., Dalton Trans. 2187 (1996)